A Novel Technique for Analysis of Electromagnetic Scattering from Microstrip Antennas of Arbitrary Shape

Savas Uckun, *Member IEEE*, Tapan K. Sarkar, *Fellow, IEEE*, Sadasiva M. Rao, *Senior Member, IEEE*, Magdalena Salazar-Palma, *Member, IEEE*

***Abstract*—A new numerical procedure is developed for the solution of the electric field integral equation (EFIE) for arbitrary-shaped microstrip structures. This approach is superior over conventional EFIE techniques particularly in the low-frequency region or where the structure to be analyzed is electrically small. A pair of new basis functions is presented which are essential to the solution in the entire frequency range of interest. The new basis functions decompose the surface current density into divergenceless and curl-free parts which essentially get decoupled at the very low end of the frequency spectrum. Typical numerical results are presented for certain examples to illustrate the difference in the results between the two methods.**

***Index Terms*—Microstrip antenna, scattering.**

I. Introduction

MUCH PROGRESS has been made in the last decade in the development of numerical solution procedures for analyzing radiation and scattering by arbitrary-shaped microstrip conducting structures [1], [2]. These procedures are primarily based on the surface equivalence principle [1] and the well-known method of moments [3] solution procedure to solve the integral equations. For conducting bodies, the solution of the electric field integral equation (EFIE), obtained by enforcing the total tangential electric-field component to zero on the metal patch, is a preferred choice. The effects of the infinite dielectric slab and the conducting plane are taken care of by the Green's function. At present, there exist many user-oriented computer codes based upon the EFIE solution, which are capable of predicting the surface currents and scattered fields accurately in the resonance region, which may be defined as the range of frequencies for which the maximum dimension of the patch is of the order of the wavelength. Although the conventional EFIE solutions are highly accurate in the resonance region, problems of inaccuracy and ill-conditioning have been reported at very low frequencies [4]. Some work has been done in this area to alleviate the ill-conditioning problem [5] but these methods are cumbersome to apply for a general arbitrarily shaped geometry.

Manuscript received February 5, 1996; revised December 24, 1996.

S. Uckun and T. K. Sarkar are with the Department of Electrical and Computer Engineering, Syracuse University, Syracuse, NY 13244-1240 USA.

S. M. Rao is with the Department of Electrical Engineering, Auburn University, Auburn, AL 36830 USA.

M. S. Salazar-Palma is with Dipartimento Señales, Sistemas y Radio Communicacion, E.T.S.I. Telecommunicacion, Polytechnique University Madrid, 28040 Madrid, Spain.

Publisher Item Identifier S 0018-9480(97)02531-3.

In this paper, an alternate method which is easily applicable to both low and resonance frequency ranges is presented. The new method is simple, efficient, accurate, and robust at all frequencies. In the present method, the authors approximate the scattering surface by planar triangular patches and define a new pair of basis functions for the method of moment solution. These basis functions decompose the surface current density into divergenceless and curl-free parts which essentially get decoupled at the very low end of the frequency spectrum. Further, these new pairs of basis functions are also used as testing functions to generate a diagonally dominant moment matrix which is well conditioned at all frequencies [4].

II. Electric Field Integral Equation (EFIE)

To solve for the radiation from arbitrarily shaped planar microstrip structures, the EFIE is utilized. In the EFIE formulation the total tangential electric field on the conducting radiating surface is equated to zero, i.e.,

$$\boldsymbol{E}_{\tan} = 0 \quad \text{on conducting patches.} \tag{1a}$$

If an equivalent current $\boldsymbol{J}_s$, on the conducting patches is assumed to exist, then

$$L(\boldsymbol{J_s}) + \boldsymbol{E}^i = 0 \quad \text{on conducting patches} \tag{1b}$$

and

$$L(\boldsymbol{J}_s) = -j\omega \boldsymbol{A} - \overline{\nabla} V \tag{2}$$

where A is the magnetic vector potential, V is the scalar potential. $\boldsymbol{E}^i$ represents the excitation. Here $L(\boldsymbol{J}_s)$ represents the electric field operator which produces an electric field due to $\boldsymbol{J}_s$. The current density $\boldsymbol{J}_s$ is situated over the infinite dielectric layer and the infinite perfectly conducting ground plane. The effects of the dielectric layer and the ground plane are treated by the Sommerfeld Green's function.

In order to solve for $\boldsymbol{J}_s$; the method of moments is applied. The triangular patches developed in [2], [5] are considered. The surface is properly triangulated, i.e., defined by an appropriate set of faces, edges, vertices, and boundary edges. Instead of the conventional triangular basis functions, the authors utilize the new basis functions. This amounts to decomposing the surface current density into divergenceless and curl-free parts which essentially get decoupled at the low end of the frequency spectrum [4].

This new approach decomposes the surface current density on triangular patches into divergenceless and curl-free parts which essentially gets decoupled at the low end of the spectrum where numerical instability sets it. This is ideally suited for electromagnetic analysis of planar microstrip structures where the antenna (generally of the order of the wavelength) is directly coupled with the feed structures (where transmission lines are electrically small in dimensions). Such a decomposition leads to a separate calculation of the contribution to the electric field due to the magnetic vector potential and the divergence of the scalar electric potential. For electrically small structures computation of $-j\omega \boldsymbol{A}$ with respect to ∇V becomes critical. The dynamic part of the electric field is primarily due to the component $\boldsymbol{A}$ which decreases with frequency, whereas the other term, ∇V increases with frequency. So even though ∇V is much larger numerically with respect to $-j\omega \boldsymbol{A}$, it is the latter term which contributes to the final result. Hence, robust numerical procedures need to be developed to solve these problems.

This is accomplished as follows. The arbitrary-shaped microstrip patch antenna is subdivided into a number of triangular patches [6] and a new set of basis functions are defined for the patch.

III. Description of the New Basis Functions

In this section, the authors describe a pair of basis functions, known as loop and patch basis functions, which are used to approximate the unknown current $\boldsymbol{J}$. The authors assume that the conducting patches are approximated by the new basis functions.

A. Loop Basis Functions

The authors consider a region of the triangulated model of the patch S as shown in Fig. 1. The authors define an elemental loop around the ith vertex by joining the centroids of the triangles and edge centers connected to the vertex i (see Fig. 1). The loop basis function for an internal vertex (i.e., vertex not situated on the boundary for an open patch) may be defined as

$$\boldsymbol{O}_i(\boldsymbol{r}) = \sum_{n_i \in \text{loop}_i} \sigma_{ni} \frac{1}{l_{ni}} \bigwedge_{ni}(\boldsymbol{R}), \qquad i = 1, 2, \cdots, E - F - B + 1 \quad (3)$$

where n_i is the edge number of the nth edge in loop i and

$$\bigwedge_n(\boldsymbol{r}) = \begin{cases} \frac{\boldsymbol{\rho}_n^{\pm}}{h_n^{\pm}}, & r \in p_n^{\pm} \\ 0, & \text{otherwise.} \end{cases} \quad (4)$$

In (3), F is the number of faces, E is the number of edges, and B is the number of boundary edges in the model. In (4), $h_n^{\pm}$ is the height of the patch $p_n^{\pm}$ from the edge n to the opposite vertex, and $\rho_n^{\pm}$ is the vector between $\boldsymbol{r}$ and the opposite vertex. The vector ρ_n^{+} is directed toward $\boldsymbol{r}$ while ρ_n^{-} is away from $\boldsymbol{r}$. $\bigwedge_{ni}$ is the usual triangular-patch basis functions defined in [1], [2]. Also note that one vertex loop must be deleted if the surface is closed.

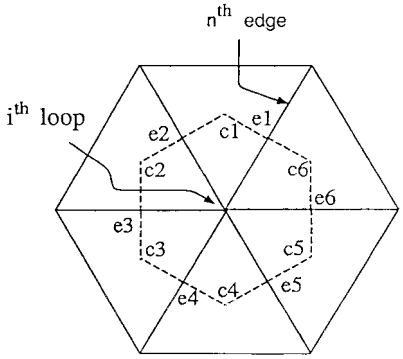

Fig. 1. Description of a loop basis function.

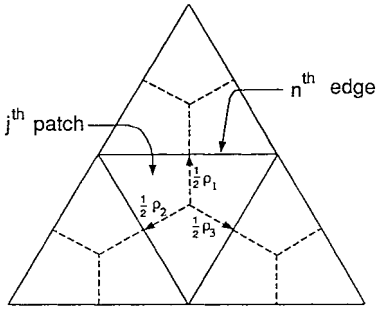

Fig. 2. Description of a patch basis function.

The term $\sigma_{ni} = \pm 1$, and is positive if the loop orientation is the same as the reference direction $\bigwedge_{ni}$ and is negative otherwise.

B. Patch Basis Functions

By referring to Fig. 2, the patch basis functions for a triangular patch j may be defined as

$$\boldsymbol{P_j}(\boldsymbol{r}) = \sum_{n_j \in \text{face}_j} \nu_{nj} \frac{1}{l_{nj}} \bigwedge_{nj}(\boldsymbol{r}), \qquad j = 1, 2, \cdots, \boldsymbol{F} - 1 \quad (5)$$

where n_j is the edge number of the nth edge of face j and $\nu_{nj} = \pm 1$ with the positive sign taken if $\bigwedge_{nj}$ is directed out of face j and the negative sign taken otherwise. l_{nj} is the length of edge n_j.

The current can thus be expanded as

$$\boldsymbol{J}(\boldsymbol{r}) = \sum_i \psi_i^{(1)} \boldsymbol{O_i}(\boldsymbol{r}) + \sum_j \psi_j^{(2)} \boldsymbol{P_j}(\boldsymbol{r}) \quad (6)$$

which represents a decomposition of the current into the divergence- and curl-free parts, respectively.

IV. Generation of the Impedance Matrix

In this section, the mathematical steps leading to the method of moment solution of the EFIE using the basis functions defined earlier is presented. The authors know that the electric field at the dielectric interface is given from a dipole of moment $\mathrm{I}\,dl$ by

$$\boldsymbol{E} = \frac{1}{j\omega 4\pi\epsilon_o} \int_l \{k_o^2[\hat{x}\mathrm{I}_x\Pi_{xx} + \hat{y}\mathrm{I}_y\Pi_{yy} + \hat{z}(\mathrm{I}_x\Pi_{zx} + \mathrm{I}_y\Pi_{zy})] \quad (7)$$

$$+\left(\hat{x}\frac{\partial}{\partial x}+\hat{y}\frac{\partial}{\partial y}+\hat{z}\frac{\partial}{\partial z}\right)\frac{\partial \mathrm{I}}{\partial l'}\Pi\gamma\Big\}\,dl$$
$$\triangleq \frac{1}{j\omega 4\pi\epsilon_o}\int_l [k_o^2 A+\nabla V]\,dl \tag{8}$$

where

$$\Pi_{xx}=\Pi_{yy}=\int_c \boldsymbol{H}_o^{(2)}(\lambda\rho)\frac{\lambda}{\boldsymbol{D}_{\mathrm{TE}}}e^{-u_o z}\,d\lambda \tag{9}$$
$$\Pi_{zx}=(\epsilon_r-1)\frac{\partial}{\partial x}\int_c \boldsymbol{H}_o^{(2)}(\lambda\rho)\frac{\lambda}{\boldsymbol{D}_{\mathrm{TE}}\cdot\boldsymbol{D}_{\mathrm{TM}}}e^{-u_o z}\,d\lambda \tag{10}$$
$$\Pi_v=\int_c \boldsymbol{H}_o^{(2)}(\lambda\rho)\frac{\lambda N}{\boldsymbol{D}_{\mathrm{TE}}\cdot\boldsymbol{D}_{\mathrm{TM}}}e^{-u_o z}\,d\lambda \tag{11}$$

and c is the contour of integration on the real axis from $-\infty$ to $+\infty$. The symbols are defined by

$$u_o=j\sqrt{k_o^2-\lambda^2} \tag{12}$$
$$u=j\sqrt{\epsilon_r k_o^2-\lambda^2} \tag{13}$$
$$\boldsymbol{D}_{\mathrm{TE}}=u_o+u\coth uh=j\sqrt{k_o^2-\lambda^2}-j\sqrt{\epsilon_r k_o^2-\lambda^2}\cot\left(\sqrt{\epsilon_r k_o^2-\lambda^2}\,h\right) \tag{14}$$
$$\boldsymbol{D}_{\mathrm{TM}}=\epsilon_r u_o+u\tanh uh=j\epsilon_r\sqrt{k_o^2-\lambda^2}-j\sqrt{\epsilon_r k_o^2-\lambda^2}\tan\left(\sqrt{\epsilon_r k_o^2-\lambda^2}\,h\right) \tag{15}$$
$$\boldsymbol{N}=u_o+u\tanh uh \tag{16}$$
$$\rho=\sqrt{(x-x')^2+(y-y')^2} \tag{17}$$

and $\hat{x}$, $\hat{y}$, and $\hat{z}$ are the unit vectors in x, y, and z directions, respectively. The tangential components of the fields at the dielectric interface are evaluated when $z=0$. In order to find the electric field distribution on an arbitrarily shaped current patch, (7) is convolved with the current distribution on the patch.

The authors utilize Galerkin's method so that the same basis functions are also used as testing functions. The authors define the usual inner product as

$$\langle f,g\rangle=\int_s f\bar{g}\,ds=\int_s fg\,ds \tag{18}$$

where the overbar represents the complex conjugate. Since g is real, the conjugate may be omitted.

With loop and patch basis functions the authors obtain

$$\langle k_o^2\boldsymbol{A}(\boldsymbol{r})+\nabla\boldsymbol{V}(\boldsymbol{r})\boldsymbol{O_p}\rangle=\boldsymbol{j}\omega 4\pi\epsilon_o\langle\boldsymbol{E^i}(\boldsymbol{r}),\boldsymbol{O_p},\rangle,\quad \text{for } p=1,2,\cdots,\boldsymbol{E}-\boldsymbol{F}-\boldsymbol{B}+1 \tag{19}$$

and

$$\langle k_o^2\boldsymbol{A}(\boldsymbol{r})+\nabla\boldsymbol{V}(\boldsymbol{r});\boldsymbol{P_q}\rangle=\boldsymbol{j}\omega 4\pi\epsilon_o\langle\boldsymbol{E^i}(\boldsymbol{r}),\boldsymbol{P_q}\rangle,\quad \text{for } q=1,2,\cdots,\boldsymbol{F}-1 \tag{20}$$

Note that in (19) since $\boldsymbol{O}_p$ is defined over a closed path, the scalar potential term ∇V term drops out of the equation. This is an important factor in determining the stability of the numerical procedure at low frequencies.

By approximating the potential and the field quantities with their respective values at centroids of the testing triangle, and

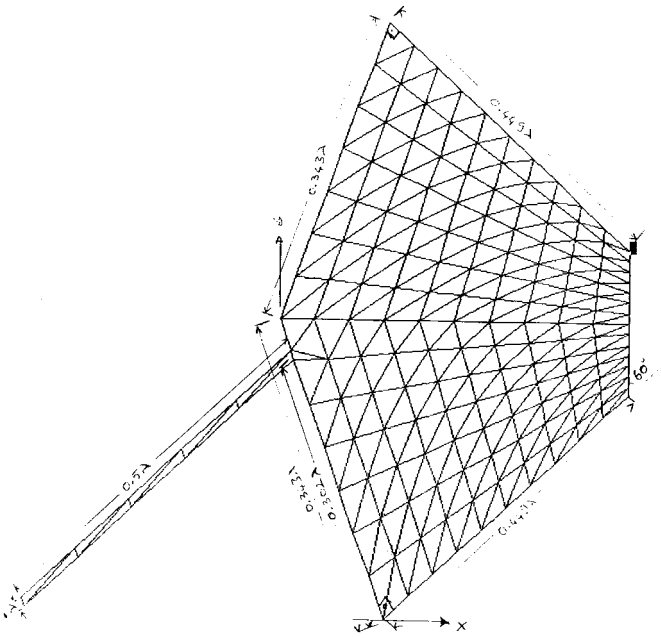

Fig. 3. A pentagonal patch antenna.

following the similar mathematical steps as in [6] the authors get the following equations:

$$\sum_{n_p\in\mathrm{loop_p}}\boldsymbol{k_o^2}\sigma_{n_p}[\boldsymbol{A}(\boldsymbol{r}_{n_p^{c+}})\cdot\rho_{n_p^{c+}}+\boldsymbol{A}(\boldsymbol{r}_{n_p^{c}-})\cdot\rho_{n_p^{c}-}]$$
$$=\boldsymbol{j}\omega 4\pi\epsilon_o\sum_{n_p\in\mathrm{loop_p}}\sigma_{n_p}[\boldsymbol{E^i}(\boldsymbol{r}_{n_p^{c+}})\cdot\rho_{n_p^{c+}}+\boldsymbol{E^i}(\boldsymbol{r}_{n_p^{c}-})\cdot\rho_{n_p^{c}-}],\quad p=1,2,\cdots,\boldsymbol{E}-\boldsymbol{F}-\boldsymbol{B}+1 \tag{21}$$

and

$$\sum_{n_q\in\mathrm{face_q}}k_o^2\nu_{n_q}[\boldsymbol{A}(\boldsymbol{r}_{n_q^{c+}})\cdot\rho_{n_q^{c+}}+\boldsymbol{A}(\boldsymbol{r}_{n_q^{c}-})\cdot\rho_{n_q^{c}-}]-\nabla^2\boldsymbol{V}(\boldsymbol{r}_q)$$
$$=\boldsymbol{j}\omega 4\pi\epsilon_o\sum_{n_q\in\mathrm{faces_q}}\nu_{nq}[\boldsymbol{E^i}(\boldsymbol{r}_{n_q^{c+}})\cdot\rho_{n_q^{c+}}+\boldsymbol{E^i}(\boldsymbol{r}_{n_q^{c}-})\cdot\rho_{n_q^{c}-}],\quad q=1,2,\cdots,\boldsymbol{F}-1 \tag{22}$$

where due to the particular choice of the basis functions the potential V_q at the qth patch is given by:

$$\nabla^2\boldsymbol{V}(\boldsymbol{r}_q)=\nabla^2\boldsymbol{V}_q=\sum_i(\boldsymbol{V}_q-\boldsymbol{V}_{qi}) \tag{23}$$

where q is the index of the qth patch, and i is the patch index of the patch adjacent to and attached to the ith nonboundary edge of patch q.

Substitution of the current expansion function given by (6) into (21) and (22), and following the derivation steps as in [6], yields a $N\times N$ system of linear equations which may be written in the following form as

$$\boldsymbol{ZI}=\boldsymbol{E} \tag{24}$$

where

$$\boldsymbol{Z}=\begin{bmatrix}\boldsymbol{Z}^{oo} & \boldsymbol{Z}^{op}\\ \boldsymbol{Z}^{po} & \boldsymbol{Z}^{pp}\end{bmatrix} \tag{25}$$
$$\boldsymbol{I}=\begin{bmatrix}\boldsymbol{I}^0\\ \boldsymbol{I}^p\end{bmatrix}\quad\text{and}\quad\boldsymbol{E}=\begin{bmatrix}\boldsymbol{E}^0\\ \boldsymbol{E}^p\end{bmatrix} \tag{26}$$

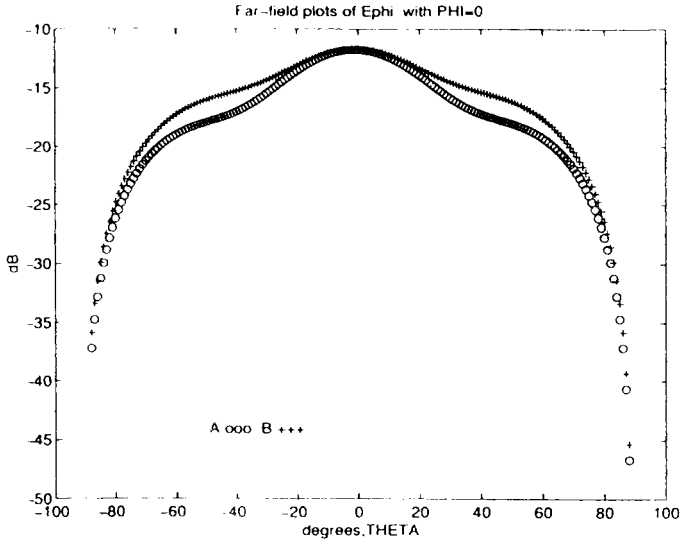

Fig. 4. 20 $\log_{10}|\boldsymbol{E}_\phi|$ at $\phi = 0$ plotted for different values of $-90^\circ \leq \theta \leq 90$.

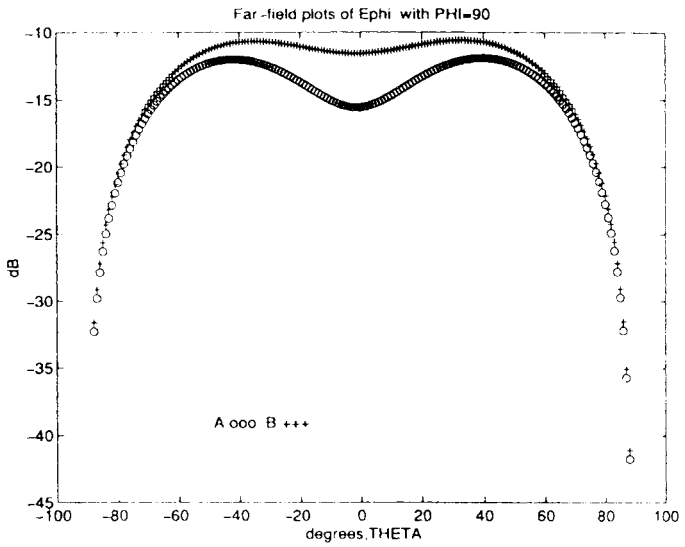

Fig. 5. 20 $\log_{10}|\boldsymbol{E}_\phi|$ at $\phi = 90$ plotted for different values of $-90^\circ \leq \theta \leq 90$.

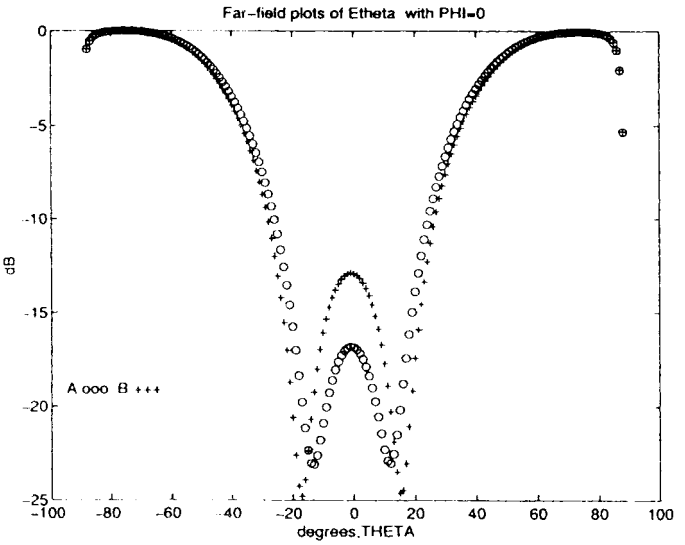

Fig. 6. 20 $\log_{10}|\boldsymbol{E}_\theta|$ at $\phi = 0$ plotted for different values of $-90^\circ \leq \theta \leq +90$.

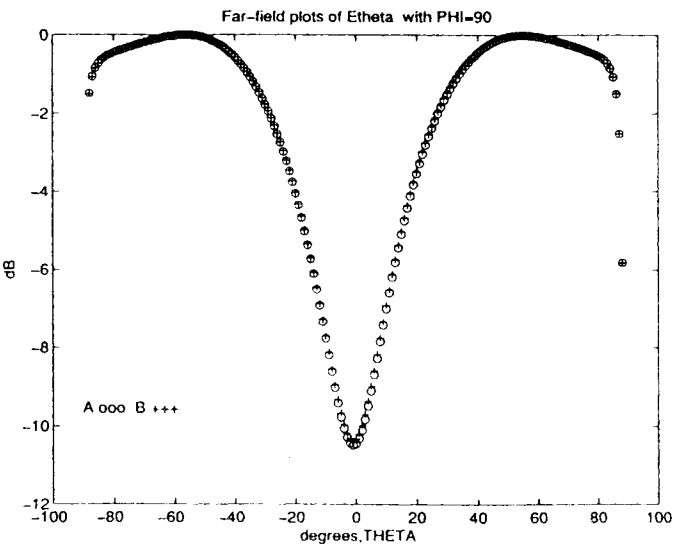

Fig. 7. 20 $\log_{10}|\boldsymbol{E}_\theta|$ at $\phi = 90$ plotted for different values of $-90^\circ \leq \theta \leq 90$.

and $\boldsymbol{Z}^{oo}$, $\boldsymbol{Z}^{op}$, $\boldsymbol{Z}^{po}$, and $\boldsymbol{Z}^{pp}$ are submatrices and $\boldsymbol{I}^o$, $\boldsymbol{I}^p$, $\boldsymbol{E}^o$, and $\boldsymbol{E}^p$ are column vectors. The elements of $\boldsymbol{Z}^{oo}$, $\boldsymbol{Z}^{op}$, $\boldsymbol{Z}^{po}$, and $\boldsymbol{Z}^{pp}$ are given by

$$\boldsymbol{Z}^{oo}_{ji} = k_o^2 \sum_{m_j \in \text{loop}_j} \sum_{n_i \in \text{loop}_i} \frac{\sigma_{m_j}\sigma_{n_i}}{l_{n_i}} \cdot [\boldsymbol{A}_{m_n^{ij+}} \cdot \rho_{m_j^{c+}} + A_{m_n^{ij-}} \cdot \rho^{c-}_{m_j}], \quad j = 1, 2, \cdots, \boldsymbol{E} - \boldsymbol{F} - \boldsymbol{B} + 1;\ i = 1, 2, \cdots, \boldsymbol{E} - \boldsymbol{F} - \boldsymbol{B} + 1 \tag{27}$$

$$\boldsymbol{Z}^{po}_{ji} = k_o^2 \sum_{m_j \in \text{face}_j} \sum_{n_i \in \text{loop}_i} \frac{\nu_{m_j}\sigma_{n_i}}{l_{n_i}} \cdot [\boldsymbol{A}_{m_n^{ij+}} \cdot \rho_{m_j^{c+}} + A_{m_n^{ij-}} \cdot \rho_{m_j^{c}-}], \quad j = 1, 2, \cdots, \boldsymbol{F} - 1; i = 1, 2, \cdots, \boldsymbol{E} - \boldsymbol{F} - \boldsymbol{B} + 1 \tag{28}$$

$$\boldsymbol{Z}^{op}_{ji} = k_o^2 \sum_{m_j \in \text{loop}_j} \sum_{n_i \in \text{face}_i} \frac{\sigma_{m_j}\nu_{n_i}}{l_{n_l}} \cdot [A^{ij+}_{mn} \cdot \rho_{m_j^{c+}} + \boldsymbol{A}^{ij-}_{mn} \cdot \rho_{m_j^{c}-}], \quad j = 1, 2, \cdots, \boldsymbol{E} - \boldsymbol{F} - \boldsymbol{B} + 1;\ i = 1, 2, \cdots, \boldsymbol{F} - 1 \tag{29}$$

and

$$\boldsymbol{Z}^{pp}_{ji} = k_o^2 \sum_{m_j \in \text{face}_j} \sum_{n_i \in \text{face}_i} \frac{\nu_{m_j}\nu_{n_i}}{l_{n_i}} \cdot [\boldsymbol{A}^{ij+}_{mn} \cdot \rho_{m_j^{c+}} + \boldsymbol{A}^{ij-}_{mn} \cdot \rho_{m_j^{c}-}] + [\boldsymbol{V}^{ij-}_{mn} - \boldsymbol{V}^{ij+}_{mn}], \quad j = 1, 2, \cdots, \boldsymbol{F} - 1, \quad i = 1, 2, \cdots, \boldsymbol{F} - 1 \tag{30}$$

where

$$\boldsymbol{A}^{ij\pm}_{mn} = \frac{\mu}{4\pi} \int_s \bigwedge_n (r') \Pi_{xx}\, dS' \tag{31}$$

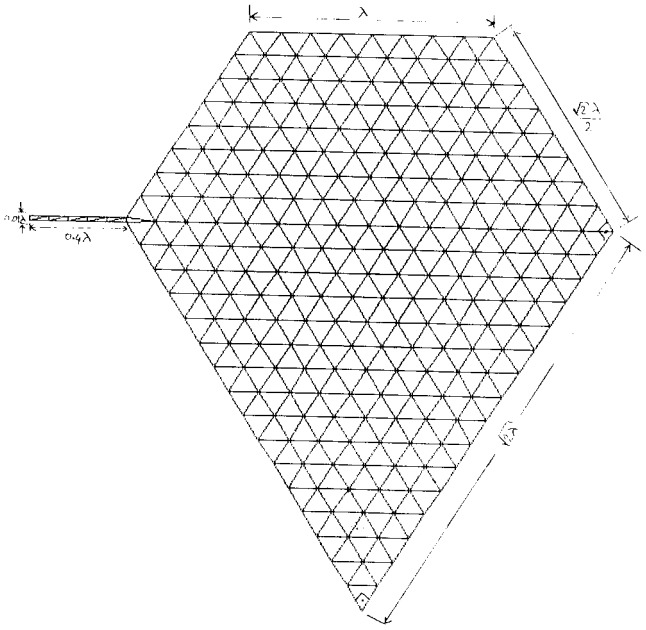

Fig. 8. A truncated square patch antenna.

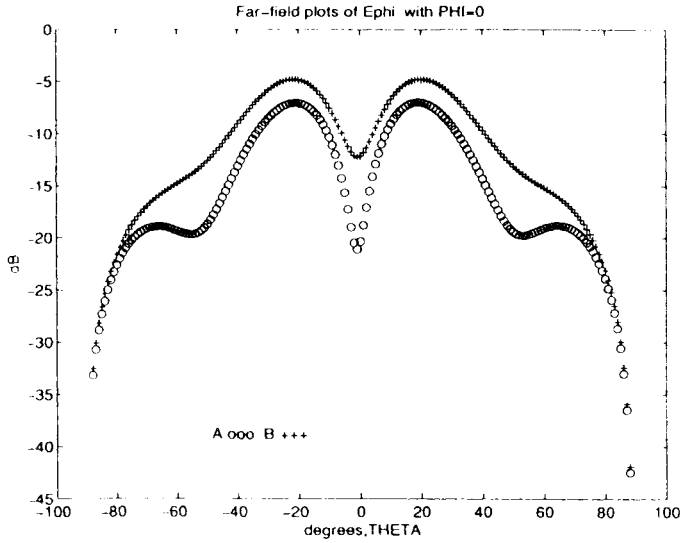

Fig. 9. 20 $\log_{10}|\boldsymbol{E}_\phi|$ at $\phi = 0$ plotted for different values of $-90^\circ \leq \theta \leq 90$.

$$\boldsymbol{V}_{mn}^{ij\pm} = \frac{j}{4\pi\omega\epsilon}\int_s \nabla_s' \cdot \bigwedge_n \Pi_v \, dS'. \tag{32}$$

For the evaluation of the potential the authors use the following:

$$\boldsymbol{R}_m^{ij\pm} = |\boldsymbol{r}_{m_j^{c\pm}} r'|. \tag{33}$$

Similarly, the element $\boldsymbol{E}^o$, and $\boldsymbol{E}^p$ are given by

$$\boldsymbol{E}_j^o = \sum_{m_j \in \text{loop}_j} [\boldsymbol{E}_{m_j^+} \cdot \rho_{m_j^{c+}} + \boldsymbol{E}_{m_j^-} \cdot \rho_{mj^{c-}}]$$
$$\text{with } j = 1, 2, \cdots, \boldsymbol{E} - \boldsymbol{F} - \boldsymbol{B} + 1 \tag{34}$$

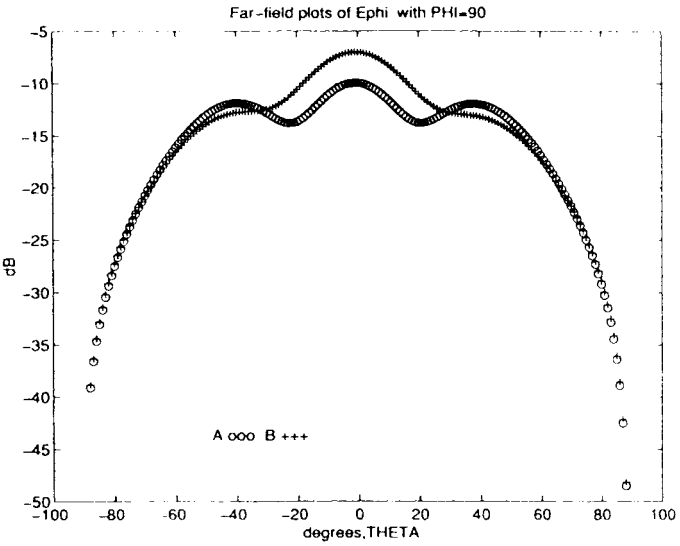

Fig. 10. 20 $\log_{10}|\boldsymbol{E}_\theta|$ at $\phi = 90$ plotted for different values of $-90^\circ \leq \theta \leq 90$.

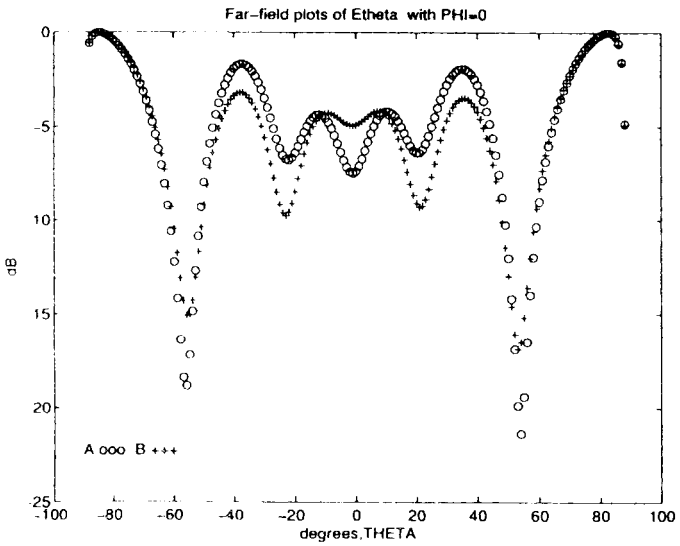

Fig. 11. 20 $\log_{10}|\boldsymbol{E}_\theta|$ at $\phi = 0$ plotted for different values of $-90^\circ \leq \theta \leq 90$.

$$\boldsymbol{E}_j^p = \sum_{m_j \in \text{patch}_j} [\boldsymbol{E}_{m_j^+} \cdot \rho_{m_j^{c+}} + \boldsymbol{E}_{m_j^-} \cdot \rho_{mj^{c-}}]$$
$$\text{with } j = 1, 2, \cdots, \boldsymbol{F} - 1 \tag{35}$$

where

$$\boldsymbol{E}_{m_j^\pm} = \boldsymbol{E}^i(r_{m_j^{c\pm}}) \tag{36}$$

The integrals appearing in (31) and (32) may be evaluated by the numerical procedures described in [1], [2]. Also, for numerical efficiency, the potential integrals should be evaluated on a face-to-face combination, as done in [2]. Then these integral values may be multiplied by appropriate constants and their contributions accumulated in the appropriate rows and columns of the moment matrix.

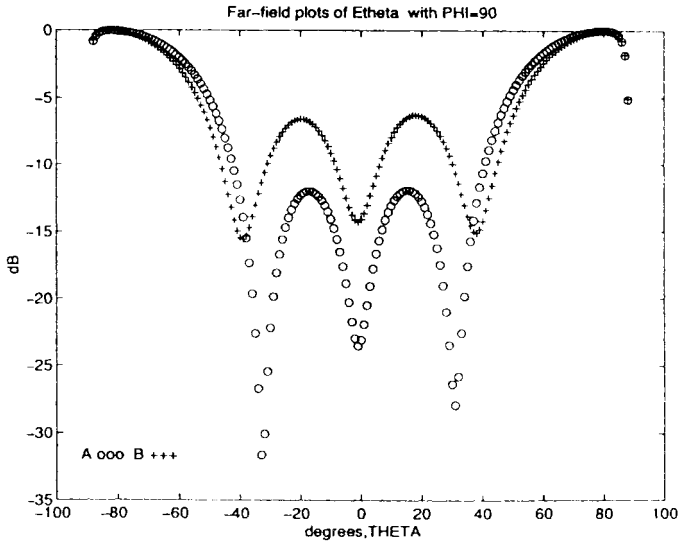

Fig. 12. 20 $\log_{10}|\boldsymbol{E}_\theta|$ at $\phi = 90$ plotted for different values of $-90^\circ \leq \theta \leq 90$.

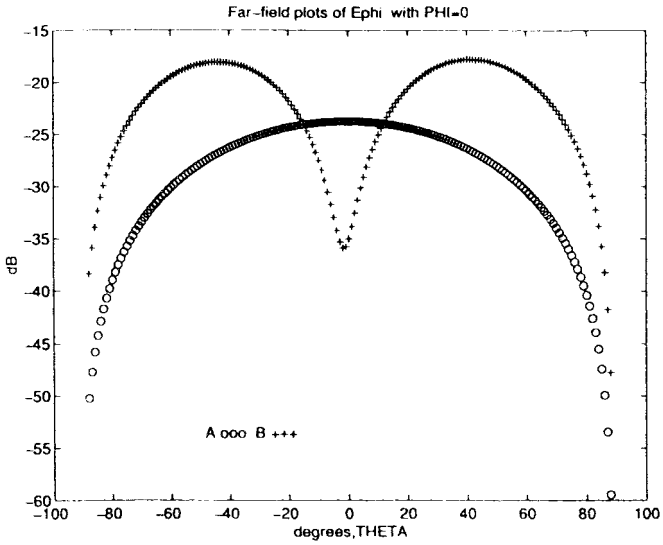

Fig. 14. 20 $\log_{10}|\boldsymbol{E}_\phi|$ at $\phi = 0$ plotted for different values of $-90^\circ \leq \theta \leq 90$.

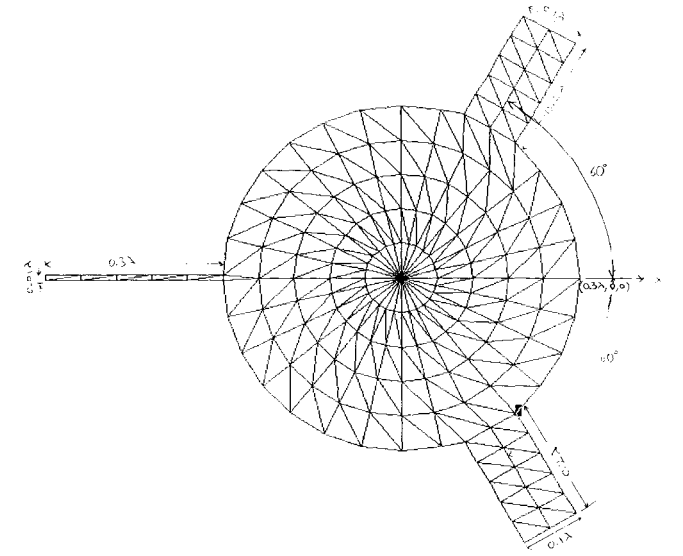

Fig. 13. A circular patch antenna with two stubs.

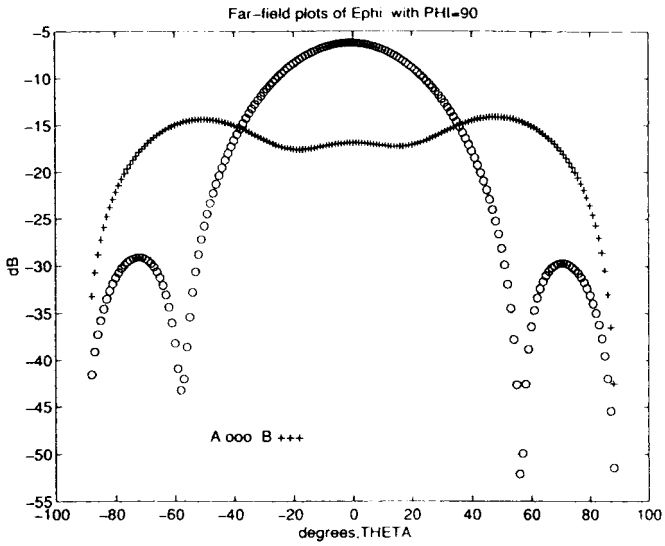

Fig. 15. 20 $\log_{10}|\boldsymbol{E}_\phi|$ at $\phi = 90$ plotted for different values of $-90^\circ \leq \theta \leq 90$.

V. Numerical Results

In this section, some numerical results are presented to illustrate the difference in the results produced by the conventional triangular patch modeling as opposed to this new procedure. For all three examples to be described, the structures are situated on an infinite dielectric slab of the complex dielectric constant $\epsilon_r = (2.62; 0.0)$ and of thickness 0.007λ.

As a first example, consider a pentagonal patch antenna of dimensions as shown in Fig. 3. The analysis was done by the new approach (marked A) as well as by the conventional approach [2] marked B. The excitation is located on the first nonboundary vertical edge at the open end of the transmission line. The results of Figs. 4–7 for the various components of the field for different angles of θ indicate that there is some differences between the two approaches. The results of the new method are somewhat different.

As a second example, consider a truncated rectangular patch antenna of $\sqrt{2}\lambda$ of a side is fed by a 0.4λ transmission vertical edge of the transmission line. The excitation is located on the first nonboundary vertical edge at the open end of the transmission line. This is shown in Fig. 8. The field patterns for the various components in Figs. 9–12 indicate that for this case, the differences between the two methods are quite large.

As a third example, consider a circular microstrip patch antenna with two stubs as shown in Fig. 13. Figs. 14–17 indicate that the new methods provide more accurate and consistent results particularly for the ϕ component of the electric field.

VI. Conclusion

A new EFIE is presented for the analysis of arbitrary-shaped microstrip structures at low frequencies of the incident

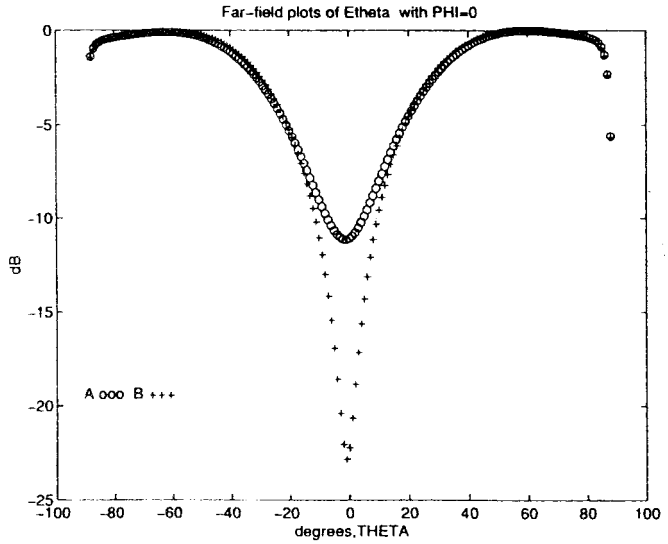

Fig. 16. $20 \log_{10}|\boldsymbol{E}_\theta|$ at $\phi = 0$ plotted for different values of $-90° \leq \theta \leq 90$.

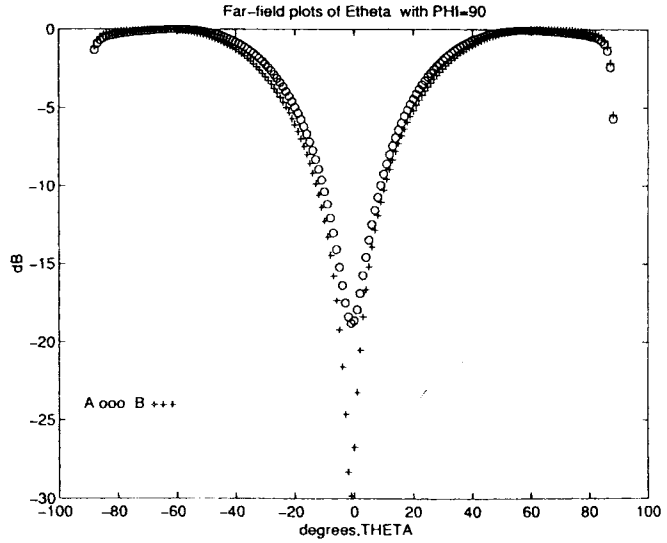

Fig. 17. $20 \log_{10}|\boldsymbol{E}_\theta|$ at $\phi = 90$ plotted for different values of $-90° \leq \theta \leq 90$.

wave or the equivalent for electrically small structures. The numerical procedure is robust, particularly for electrically small structures, and of the same order of efficiency as that of the earlier methods. Crucial to the formulation is the development of a new set of basis functions which decompose the surface current density into curl-free and divergenceless parts. Typical numerical results are presented to illustrate the applicability of the new method. Comparisons of the numerical values with previous computations have been made and results have been presented only for those cases where differences have been observed.

REFERENCES

[1] K. A. Michalski and S. Zhang, "Electromagnetic scattering and radiation by surfaces of arbitrary shape in layered media, Part I: Theory," *IEEE Trans. Antennas Propagat.*, vol. 38, pp. 335–344, Mar. 1990.
[2] T. K. Sarkar, P. Midya, Z. Maricevic, M. Kahrizi, S. M. Rao, and A. R. Djordjevic, "Analysis of arbitrarily shaped microstrip patch antennas using the sommerfeld formulation," *Int. J. Microwave and Millimeter-Wave Comput.-aided Eng.*, vol. 2, no. 3, pp. 168–178, 1992.
[3] R. F. Harrington, *Field Computation by Moment Methods*. New York: Macmillan, 1968.
[4] D. R. Wilton, J. S. Lin, and S. M. Rao, "A novel technique to calculate the electromagnetic scattering by surfaces of arbitrary shape," submitted for publication.
[5] J. R. Mautz and R. F. Harrington, "An improved E-field solution for a conducting body of revolution," *AËU*, vol. 36, pp. 198–206, May 1962.

Savas Uckun (S'93–M'95) was born in Gaziantep, Turkey, on July 18, 1956. He received the B.Sc. degree in electrical engineering, from the Middle East Technical University (METU), Gaziantep Engineering Faculty, Gaziantep, Turkey, in 1980, the M.Sc. degree in electrical engineering from METU, in 1983, a second M.Sc. degree in computer science from the State University of New York, at Albany, in 1987, and the Ph.D. degree in electrical engineering from METU in 1992.

He served on the electrical engineering faculty of METU as a Research Assistant from 1980 to 1984, where he is currently a Lecturer. From June 1995 to September 1995 he was with the Department of Electrical Engineering, Syracuse University, Syracuse, NY, as a visiting Assistant Professor.

Tapan K. Sarkar (S'69–M'76–SM'81–F'92), photograph and biography not available at the time of publication.

Sadasiva M. Rao (M'83–SM'90), photograph and biography not available at time of publication.

Magdalena Salazar-Palma (M'89) was born in Granada, Spain. She received the Ingeniero Superior and Doctor Ingeniero degrees in telecommunication engineering from the Universidad Politécnica de Madrid, Madrid, Spain.

She is a professor (Professor Titular) in the Signals, Systems and Radiocommunications Department at the Escuela Técnica Superior de Ingenieros de Telecomunicación, Universidad Politécnica de Madrid. Here interests are focused on electromagnetic field theory, computational and numerical methods for microwave structures and passive components analysis, as well as on hybrid and monolithic microwave integrated circuits.